Hydrodynamic origin for the suspension viscoelasticity of rough colloids

Shravan Pradeep, Alan Wessel and Lilian C. Hsiao

Citation: Journal of Rheology **66**, 895 (2022); doi: 10.1122/8.0000424
View online: https://doi.org/10.1122/8.0000424
View Table of Contents: https://sor.scitation.org/toc/jor/66/5
Published by the The Society of Rheology

Hydrodynamic origin for the suspension viscoelasticity of rough colloids

Shravan Pradeep,[a] Alan Wessel, and Lilian C. Hsiao[b]

Department of Chemical and Biomolecular Engineering, North Carolina State University, Raleigh, North Carolina 27695

(Received 19 December 2021; final revision received 7 July 2022; published 11 August 2022)

Abstract

We report the linear rheology for dense suspensions of sterically stabilized smooth and mesoscopically rough colloids interacting as hard particles. Small amplitude oscillatory measurements reveal that rough colloids at high volume fractions exhibit storage and loss moduli that are orders of magnitude greater than smooth colloids. Frequency-concentration superposition is used to collapse the viscoelasticity data onto a master curve, where shift factors suggest a more elastic microstructure and reduced cage volume for rough particles. A combination of the mode-coupling theory, hydrodynamic modeling, and the activated hopping theory shows that these rough particles with significantly reduced localization lengths tend to become trapped in their glassy cages for extended periods of time. High-frequency data show that rough colloids, but not smooth colloids, display a transition from a free-draining to a fully lubricated state above the crossover volume fraction and, furthermore, exhibit solidlike behavior. Scaling analyses support the idea that lubrication forces between interlocking asperities are enhanced, leading to rotational constraints and stress-bearing structures that significantly elevate the viscoelasticity of dense suspensions. The results provide a framework for how particle surface topology affects the linear rheology in applications such as coatings, cement, consumer products, and shock-absorbing materials. https://doi.org/10.1122/8.0000424

I. INTRODUCTION

Understanding how mesoscale particle roughness affects suspension rheology is an important problem because most technologically relevant materials contain particulates with anisotropic surfaces. Dense suspensions of such particulates are used in energy-efficient batteries, gas and oil processing, the agricultural and food sectors, as well as pharmaceutical and consumer formulations. Studies that move beyond hard spheres and scientifically investigate rheological effects are now possible due to recent progress in synthesis methods that produce well-controlled particle roughness [1]. In this study, we focus on the linear viscoelastic properties of dense colloidal suspensions, which are consequences of the interplay between the Brownian and hydrodynamic forces between neighboring particles that form dynamically arrested cages. These excluded volume effects depend on the colloid volume fraction (ϕ) and the nature of the interparticle forces [2]. At low to moderate volume fractions ($\phi < 0.30$), colloidal suspensions display stresses due to contributions from the solvent viscosity, the Brownian motion, and particle interactions with one another [3]. As ϕ increases, the environment around hard colloids becomes crowded, and the Brownian motion is slowed by lubrication hydrodynamics [4–6] as well as by any irregularities in the particle geometry [7–10]. The kinetic arrest results in an increase in the suspension stress, and understanding how particle crowding affects bulk stresses is important in fields ranging from cancer cell dynamics [11] to the prediction of geological phenomena [12]. Here, we are especially interested in how colloid surface roughness affects the frequency (ω)-dependent linear oscillatory rheology of dense colloidal suspensions.

The slow dynamics and finite viscoelasticity of dense suspensions are a result of collective kinetic trapping by nearest neighbors. When suspensions are dilute ($\phi < 0.05$), colloidal dynamics are readily described by the Stokes–Einstein–Sutherland relation, which states that the translational self-diffusivity of a colloid is $D_0 = k_B T/6\pi\eta_s a$, where $k_B T$ is the thermal energy, a is the particle radius, and η_s is the solvent viscosity. As ϕ approaches the glass transition point ($\phi_g \approx 0.58$ for hard spheres), deviation from Fickian diffusion manifests as a sublinear regime in the mean-squared displacement at intermediate lag times. This regime separates two diffusive dynamics: the short-time β-relaxation mode arises from particle rearrangement inside the ϕ-dependent cage defined by a colloid's nearest neighbors, while the long-time α-relaxation mode is a consequence of slow cage rearrangement events that vanishes near random close packing ($\phi_{max} = 0.64$ for hard spheres) [5]. Both relaxation modes are well established in experiments and computer simulations for colloidal hard spheres at $\phi < 0.55$ [5,6] but are much less understood for particles that deviate from hard spheres or at high ϕ – the subject of this study.

The translational diffusion coefficients are typically much more strongly affected by ϕ than their rotational counterparts, primarily due to the minimal effects of hydrodynamics on the rotational mode of a smooth spherical particle. However, this statement does not necessarily hold true for rough colloids suspended at high ϕ, where the surface asperities between nearest neighbors generate rotational constraints [13,14]. Such types of rough colloids shear thicken strongly [15,16], tend to suppress crystallization [17], and form

[a]Present address: Department of Earth and Environment Sciences, University of Pennsylvania, Philadelphia, PA 19104.
[b]Author to whom correspondence should be addressed; electronic mail: lilian_hsiao@ncsu.edu

stringlike networks when used in depletion flocculated gels [17]. The microscopic origin of their unusual material properties is attributed to the presence of surface asperities. When two rough colloids are sufficiently near one another, the asperities are able to interlock and impart a tangential resistance that is not accessible with smooth spheres [13,18,19]. Earlier, we observed that the rotational dynamics of rough colloids in a quiescent suspension is much slower than that of smooth colloids, even though the microstructure and translational mobility are relatively unchanged [10]. Collectively, these observations suggest that both the storage and loss moduli (G' and G'') of dense suspensions comprising rough colloids could be different from that displayed by classical hard sphere systems because of the enhanced hydrodynamic interactions between nearest surface asperities [13,19].

The contributions of cage relaxation and lubrication hydrodynamics to the suspension viscoelasticity can be modeled using the mode-coupling theory (MCT) combined with equations of motion that account for diffusional boundary layers and hydrodynamic interactions. MCT is a dynamic mean-field approach that was originally developed to predict the glass transition and subsequently applied to colloidal glass rheology [20–22]. Specifically, it predicts the change in single-particle dynamics due to particle caging [20]. Incorporation of an ensemble-averaged localization parameter, which can be thought of as the characteristic length scale of microscopic cage hopping, into Green–Kubo transport equations generates a prediction of the glassy elastic modulus [23]. One of the mechanisms for the slow diffusion in this caging regime comes from activated processes in colloidal glasses. The probability for particles to "hop" over an entropic barrier and move outside of its cage is a function of the barrier height and the diffusion length scale. The size of transient cages formed in the glassy regime of colloidal suspensions is directly related to the localization length. In addition to microstructural interactions, when a dense suspension of hard spheres is sheared at high oscillatory frequencies ω, lubrication interactions dominate over diffusion and a high-frequency G' plateau is observed with a scaling that is independent of the applied frequency ($G' \sim \omega^0$). In contrast, a freely draining system with screened lubrication interactions will not develop a high-frequency plateau but rather exhibit a power-law dependence ($G' \sim \omega^{1/2}$) [24]. These type of measurements have been made using specialized high-frequency torsional devices [2,25] or standard rheometers [26,27] if the particle size and Brownian time scale is sufficiently large.

At $\phi \geq \phi_g$, sterically stabilized silica and poly(12-hydroxystearic acid) stabilized poly(methyl methacrylate) (PHSA-PMMA) colloids have traditionally shown scalings of $G' \sim \omega^{1/2}$, unless the stabilizer chain lengths are long or if surface asperities are present. Schroyen *et al.* showed that when the PHSA brush length is large compared to the particle size ($h_c = 60$ nm, $h_c/2a = 0.08$, where h_c is the PHSA contour length), brush compression suppresses free-draining behavior, increases the viscous contribution to the suspension stress, and causes the lubrication regime to shift to extremely high frequencies. The so-called "hairy" PHSA-PMMA particles exhibit screened lubrication interactions at moderate ω, unlike classical silica and PHSA-PMMA hard spheres with thin stabilizer layers ($h_c \sim 10$ nm). They also showed that the diffusive boundary layer thickness for raspberrylike silica colloids decreases with ϕ, possibly due to the reduced space for fluid flow at very small separation distances between surface asperities [2].

In this work, we investigate G' and G'' of smooth and rough PHSA-PMMA colloids and their frequency-dependent linear rheology. The colloids are synthesized using free radical polymerization and suspended at different volume fractions in a refractive index-matched solvent, squalene, that minimizes van der Waals interactions and generates hard-particle interactions. Small amplitude oscillatory strain sweeps are first used to identify the linear viscoelastic regime for all suspensions. Then, frequency sweeps at a fixed strain are used to perturb the microstructure of the suspensions. The resultant data are modeled using MCT and hydrodynamic models [28] to deduce how surface morphology alters the localization length and lubrication interactions of rough colloids. Shift factors are used to collapse the frequency sweep data onto a master curve, where the magnitude of the shift factors is used to infer the microstructure and relaxation time scales of rough colloids. A ϕ-dependent caging length scale, obtained from the glassy elastic modulus and the dynamic localization theory, provides further physical insight into why the viscoelasticity of rough colloids differs significantly from their smooth counterparts in dense suspensions.

II. MATERIALS AND METHODS

A. Colloidal synthesis and characterization

Smooth PHSA-PMMA microspheres are synthesized using dispersion polymerization of PHSA-(glycidyl methacrylate)-(methyl methacrylate) (PHSA-GMA-MMA) block copolymer with 2-azobisisobutyronitrile (AIBN) as the free radical initiator and MMA and methacrylic acid as the monomer mixture. The fluorescent dye Nile red is added during the synthesis reaction to enable characterization of the colloidal volume fraction using confocal laser scanning microscopy. Rough PHSA-PMMA colloids are synthesized by adding a cross-linker, ethylene glycol dimethacrylate (EGDMA), near the start of the dispersion polymerization reaction after the particle seeding commences. Earlier studies indicate that the PHSA copolymer brush is 10–15 nm in contour length with standard reaction protocols, as detailed elsewhere [29]. The synthesized particles are initially stored in a stock solution of hexane and later transferred to an index-matching solvent, squalene ($n_{\text{squalene}} = n_{\text{PMMA}} = 1.49$, $\rho_{\text{squalene}} = 858\ \text{kg/m}^3$, $\rho_{\text{PMMA}} \approx 1180\ \text{kg/m}^3$) at $0.45 \leq \phi \leq 0.62$. The density difference between the particles and the solvent is neglected due to the slow sedimentation rate at high volume fractions and the relatively short time for rheological testing.

Colloidal particles swell in squalene because of polymer-solvent interactions. The effective swollen particle diameter ($2a_{\text{eff}}$) of both smooth and rough colloids is obtained from 2D confocal microscopy images of colloids suspended in the solvent. Images are collected near the bottom of the sample vials where colloids form a single layer. The images are used to obtain particle sizes and the 2D circularity parameter (Ψ_{2D}) from 100 independent particles for each type of surface morphology. The effective diameters, $2a_{\text{eff}}$, for suspended colloidal particles are obtained using the expression

$a_{\text{eff}} = (A_P/\pi)^{1/2}$. The values of $2a_{\text{eff}}$ are $1.50\,\mu\text{m} \pm 4\%$ for smooth colloids and $1.55\,\mu\text{m} \pm 5\%$ for rough colloids. For comparison, representative scanning electron micrographs of the dry particles are shown in Fig. 1. The parameter Ψ_{2D} represents the deviation of a shape from a circle and is mathematically defined as the ratio of area to the square of the particle perimeter as $\Psi_{2D} = 4\pi A_P/P_P^2$, where A_P is the maximum 2D area of the particle and P_P is the corresponding perimeter. The Ψ_{2D} value is 0.99 ± 0.01 for smooth colloids and 0.87 ± 0.03 for rough colloids.

Centrifugation of PMMA in squalene at gravitational stress equivalent to $1500\,g$ is used to obtain dense sediments at random close packing (ϕ_{RCP}). The high speed of centrifugation reduces the chances of crystallization by rapidly quenching the system [30]. Excess solvent is removed from the centrifuged sediment, and an appropriate volume is re-added to the sediment followed by slowly rolling the samples over a period of days to obtain the required ϕ. The suspensions are imaged on a confocal laser scanning microscope (Leica SP8) to obtain the particle volume fraction, $\phi = 4\pi a_{\text{eff}}^3 N_P/V_{\text{box}}$, where N_P is the number of particle centroids identified using standard image processing routines [31] in a 3D image volume, V_{box}. Additionally, we estimate the maximum packing ϕ_{max} of our PHSA-PMMA colloidal suspensions through confocal imaging of the sediments, which are undisturbed over a period of three months. Using this method, we find that $\phi_{\text{max,S}} = 0.64$ for the smooth colloids (equivalent to ϕ_{RCP} for frictionless, monodisperse spheres [32]) and $\phi_{\text{max,R}} = 0.57$ for the rough colloids used in this study. The reduction in ϕ_{max} for rough colloids is likely due to their hindered rotational dynamics [15,16]. Because smooth and rough colloids have different values of ϕ_{max}, we use the jamming distance parameter, $\Delta\phi/\phi_{\text{max}} = (\phi_{\text{max}} - \phi)/\phi_{\text{max}}$, to normalize the volume fraction for a better comparison of their rheological differences.

B. Rheological measurements

A stress-controlled rheometer (TA Instruments, DHR-2) equipped with a 50 mm sand-blasted cone and plate geometry is used to perform oscillatory strain sweep experiments where the strain γ varies from 0.01% to 100% at a fixed frequency $\omega = 1$ rad/s. Small amplitude oscillatory frequency sweep experiments are conducted in the linear viscoelastic regime at γ values below the yield strain. After sample loading and prior to the beginning of data collection, samples are allowed to equilibrate for 60 s to remove prior shear-induced microstructural changes. To reduce the dilatancy tendencies of the suspensions during sample loading, the cone geometry is lowered very slowly at a constant rate of 10 micro.m/s, while the axial force is monitored continuously to ensure that it does not exceed the instrument limits.

III. RESULTS AND DISCUSSION

A. Linear viscoelastic measurements

Strain sweep experiments performed on suspensions of smooth ($0.45 \le \phi \le 0.62$) and rough ($0.45 \le \phi \le 0.55$) colloids show that the G' and G'' remain independent of the applied strain when $\gamma < 10\%$, followed by the onset of nonlinearity and yielding (Fig. 2). For suspensions of smooth colloids, the γ values at the onset of nonlinearity and yielding decrease with increasing ϕ, similar to earlier results reported in the literature [28,33,34]. In contrast, this observation is not as clear in suspensions of rough colloids. One plausible explanation is that the rough particles experience rotational constraints at $\phi \ge 0.53$, which could produce clusters that do not significantly change in size with increasing ϕ and, therefore, the linearity limit to remain constant above ϕ_c [35]. In contrast, the linearity limit decreases with increasing ϕ for smooth colloids, which may indicate larger rigid clusters connected by weaker intercluster bonds. For both types of particles at $\phi \le 0.50$, the G' values are always lower than the G'' values; suspensions of smooth colloids at $\phi \le 0.55$ and rough colloids at $\phi \le 0.52$ exhibit liquidlike behavior. This result is also similar to the data for silica colloids dispersed in ethylene glycol [28]. At higher ϕ, suspensions of smooth colloids ($\phi \ge 0.58$) and rough colloids ($\phi \ge 0.53$) become solidlike with $G' > G''$. A major difference is that both the G' and G'' values of rough colloids at $\phi \ge 0.53$ are nearly 10^3 times that observed in suspensions of smooth colloids at the highest volume fraction ($\phi = 0.62$).

Figure 3 shows changes in G' and G'' as a function of ω for smooth colloids. At $\phi = 0.45$ and $\omega > 10$ rad/s, the suspension behaves as a fluid for which $G' \sim \omega^2$ and $G'' \sim \omega$. This fluid behavior changes to a solidlike behavior at $\phi \ge 0.58$ where $G' > G''$ at $\omega \le 1$ rad/s. There are two crossover points observable or inferable at low and high frequencies (especially, apparent for $\phi = 0.53$), corresponding to the long-time (out-of-cage) and short-time (in-cage) relaxation time scales. As ϕ increases from 0.45 to 0.62, the magnitudes of G' and G'' increase by one to two orders of magnitude, with G' increasing more than G'', which indicates the formation of confining cages. The relaxation frequencies also shift to lower frequencies as ϕ increases, qualitatively indicating that it takes longer for colloidal particles to escape from their cages. A more quantitative measure obtained using MCT will be discussed in Sec. III D.

The frequency dependence of G' and G'' for suspensions of rough colloids is shown in Fig. 4. Rough colloids suspended at $\phi \le 0.52$ exhibit qualitatively similar fluidlike behavior as the smooth colloids at $\phi \le 0.58$. The most interesting observation is the dramatic increase in G' and G'' at $\phi \ge 0.53$. The G' value becomes frequency independent, reminiscent of a high-frequency plateau modulus observed in compressed emulsions [36] and arrested gel networks [37–39]. For rough colloids at $\phi = 0.53$, the magnitude of G' is 10^2–10^3 times higher than that of smooth colloids while the magnitude of G'' is only 10^0–10^1 times higher, consistent with the strain sweep experiments. Another interesting difference is the appearance of a reproducible G'' minimum at $\omega \approx 1$ rad/s, which is a phenomenon often observed in glassy suspensions [40]. When $\phi = 0.56$, the magnitudes of both G' and G'' for rough colloids are much larger than their smooth counterparts, suggesting that both the elastic contribution from the glassy structure and the viscous dissipation between surface asperities increase significantly. The relative contributions of both dissipation modes for rough colloids are examined in greater detail in Sec. III D.

In both suspensions of smooth and rough colloids at $\phi < 0.50$, the frequency-dependent linear viscoelastic moduli

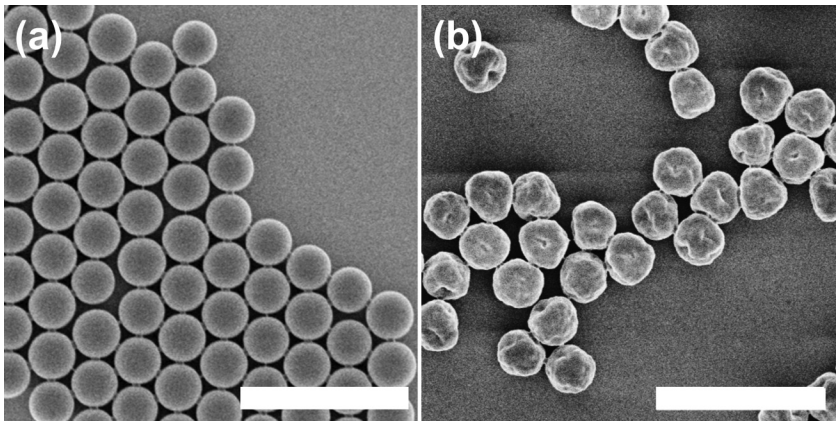

FIG. 1. Representative scanning electron micrographs of (a) smooth and (b) mesoscopically rough PHSA-PMMA colloids. Scale bars = 5 μm.

scale is characteristic of suspensions with liquidlike behavior, shown using a simple Maxwell model fitted to the rheological data in Sec. III C. For suspension at $\phi \geq 0.50$, the increase in particle concentration results in modified particle dynamics and an increase in relaxation time scales due to particle caging effects, which requires a different model to model the viscoelastic behavior. Section III D uses an MCT-based model that captures the high-frequency rheological data to provide physical insight into the differences between smooth and rough colloids.

B. Rationale for estimating the crossover point ϕ_c

To estimate the ϕ at which the suspensions begin to exhibit kinetic arrest and glassy dynamics, we plot G' and G'' at fixed ω values as a function of ϕ, in order to determine the crossover volume fraction ϕ_c [41]. The value of ϕ_c is a mechanical descriptor of the microstructural rigidity, and we estimate ϕ_c from the amplitude sweep for the colloidal suspensions, where G' crosses G'' as ϕ is increased. Figure 5 shows the data for smooth and rough colloids at two different frequencies ($\omega = 1$, 10 rad/s). The data indicate that $\phi_c = 0.58$ for smooth colloids and $\phi_c = 0.53$ for rough colloids, independent of ω. The value of ϕ_c for smooth colloids coincides with the glass transition point predicted for suspensions of hard spheres [23].

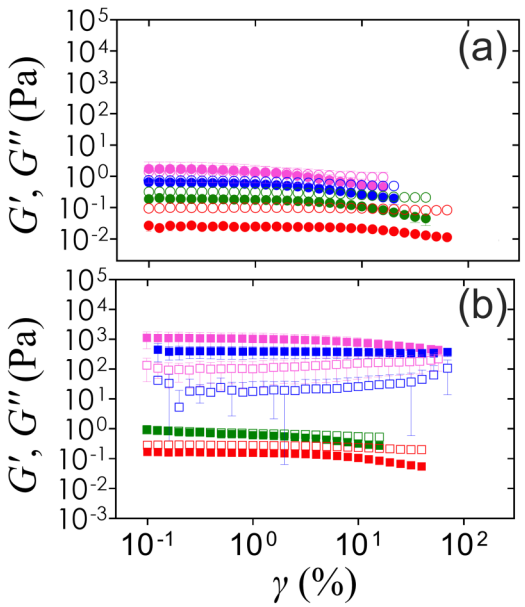

FIG. 2. Strain sweeps of suspensions containing (a) smooth (circles) and (b) rough particles (squares). The values of G' (closed symbols) and G'' (open symbols) are plotted as a function of the applied γ. Experiments are performed at $\omega = 1$ rad/s. Volume fractions indicated for the smooth particle suspensions in (a) are $\phi = 0.45$ ($\Delta\phi/\phi_{max} = 0.30$, red), $\phi = 0.55$ ($\Delta\phi/\phi_{max} = 0.14$, green), $\phi = 0.58$ ($\Delta\phi/\phi_{max} = 0.09$,blue), and $\phi = 0.62$ ($\Delta\phi/\phi_{max} = 0.03$, purple). Volume fractions indicated for the rough particle suspensions in (b) are $\phi = 0.45$ ($\Delta\phi/\phi_{max} = 0.21$, red), $\phi = 0.52$ ($\Delta\phi/\phi_{max} = 0.09$, green), $\phi = 0.53$ ($\Delta\phi/\phi_{max} = 0.07$, red), and $\phi = 0.56$ ($\Delta\phi/\phi_{max} = 0.02$, purple).

C. Maxwell model description for $\phi < 0.50$

The viscoelastic moduli for suspensions of smooth and rough colloids at $\phi = 0.45$ are shown in Fig. 6. For all ω, the

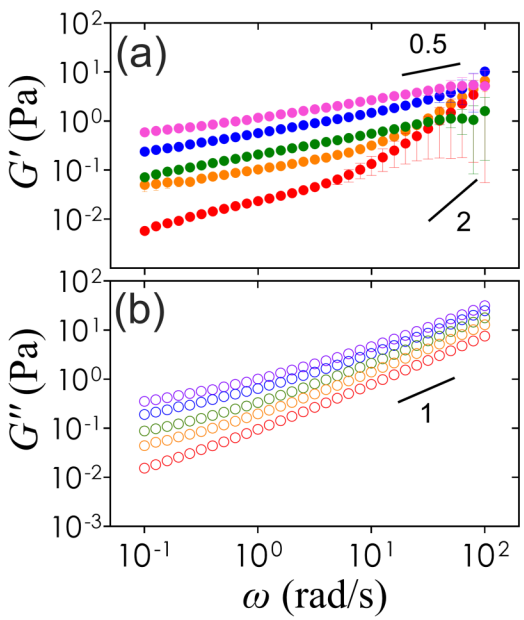

FIG. 3. Frequency sweeps of suspensions containing smooth particles. The values of (a) G' (closed symbols) and (b) G'' (open symbols) are plotted as a function of the applied ω. Experiments are performed in the linear viscoelastic regime. Volume fractions are $\phi = 0.45$ ($\Delta\phi/\phi_{max} = 0.30$, red), $\phi = 0.53$ ($\Delta\phi/\phi_{max} = 0.18$, orange), $\phi = 0.55$ ($\Delta\phi/\phi_{max} = 0.14$, green), $\phi = 0.58$ ($\Delta\phi/\phi_{max} = 0.09$, blue), and $\phi = 0.62$ ($\Delta\phi/\phi_{max} = 0.03$, purple).

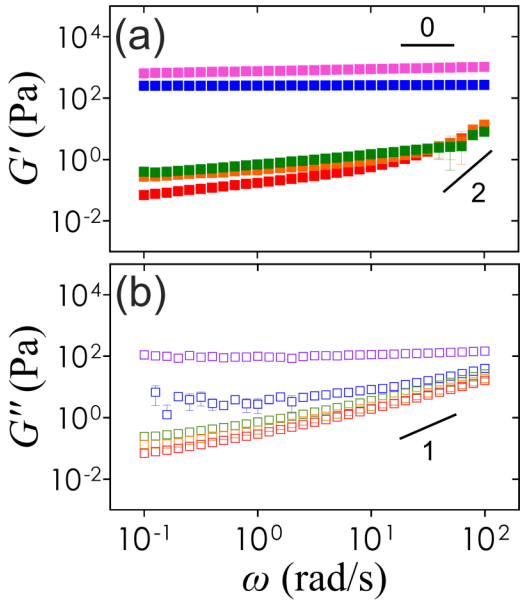

FIG. 4. Frequency sweeps of suspensions containing rough particles. The values of (a) G' (closed symbols) and (b) G'' (open symbols) are plotted as a function of the applied ω. Experiments are performed within the linear regime. Volume fractions are $\phi = 0.45$ ($\Delta\phi/\phi_{max} = 0.21$, red), $\phi = 0.50$ ($\Delta\phi/\phi_{max} = 0.12$, orange), $\phi = 0.52$ ($\Delta\phi/\phi_{max} = 0.09$, green), $\phi = 0.53$ ($\Delta\phi/\phi_{max} = 0.07$, blue), and $\phi = 0.56$ ($\Delta\phi/\phi_{max} = 0.02$, purple).

loss moduli exhibit a single scaling of $G'' \sim \omega$. The storage moduli do not exhibit a uniform scaling below $\omega < 10$ rad/s, but beyond $\omega > 10$ rad/s, a single form $G' \sim \omega^2$ is obtained for both particle types at the same ϕ. Thus, at $\omega > 10$ rad/s, both types of suspensions at $\phi = 0.45$ behave as viscoelastic fluids. For small amplitude oscillatory experiments, the frequency dependencies of the viscoelastic shear moduli (G'

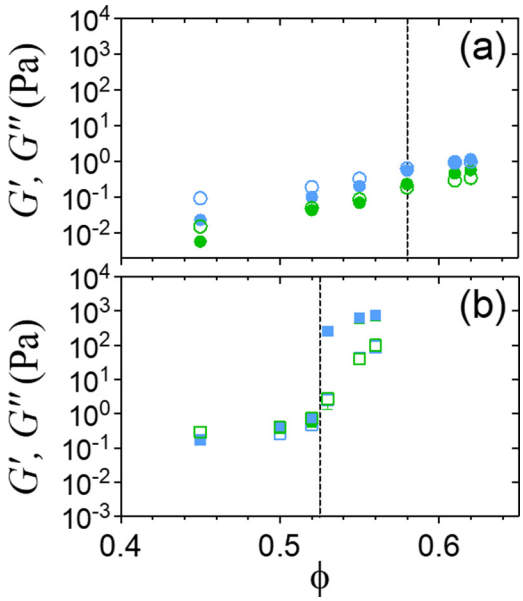

FIG. 5. Crossover volume fraction. The values of G' (closed symbols) and G'' (open symbols) for (a) smooth and (b) rough colloids are plotted as a function of ϕ. Data from two different frequencies are shown: $\omega = 1$ rad/s (green) and $\omega = 10$ rad/s (blue). Dashed lines represent ϕ_c where G' and G'' intersect.

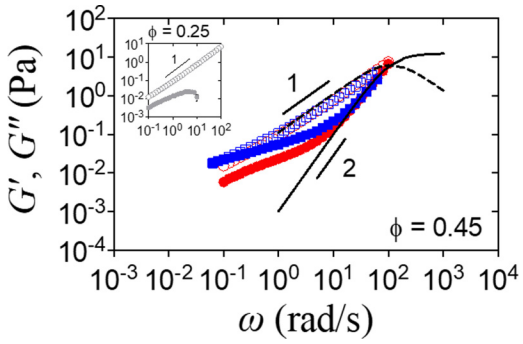

FIG. 6. Maxwell model fit for suspensions at moderate ϕ. Values of G' (closed symbols) and G'' (open symbols of smooth (circles) and rough (squares) colloids plotted as a function of ω at $\phi = 0.45$. Solid and dashed lines are Maxwell models for G' and G'' respectively. *Inset*: Viscoelastic moduli as a function of ω for smooth colloids at $\phi = 0.25$.

and G'') are described by the Maxwell model as [42]

$$G'(\omega) = G\frac{(\omega\tau_{rel})^2}{1 + (\omega\tau_{rel})^2}, \tag{1}$$

$$G''(\omega) = G\frac{\omega\tau_{rel}}{1 + (\omega\tau_{rel})^2}. \tag{2}$$

Here, G is the relaxation modulus (Pascal) and τ_{rel} is the timescale of relaxation (second), which is the inverse of the crossover frequency. The fit values used in Fig. 6 are $G = 12.5$ Pa and $\tau_{rel} = 0.009$ s for both types of suspensions at $\phi = 0.45$. The frequency-dependent viscoelastic moduli of smooth and rough colloids fall on the same curve as the Maxwell model at $\omega > 1$ rad/s. Furthermore, at 10 rad/s $< \omega <$ 100 rad/s, both types of suspensions display expected liquidlike scaling with $G' \sim \omega^2$ and $G'' \sim \omega$. At $\omega < 1$ rad/s, rough colloids have a slightly higher G' than that of smooth colloids, and there is a second crossover point between G' and G'' for the rough particles ($\tau_{rel} = 10$ s). There is little difference in the viscoelastic behavior between suspensions of smooth and rough particles at $\phi < 0.50$. For $\phi < 0.50$, the surface roughness does not affect the rheology in the "high-frequency regime." The reason why we chose a Maxwell model and not MCT to fit the data for $\phi = 0.45$ in Fig. 6 is because of the lack of a measurable crossover between G' and G'' at low ω for smooth colloids, representing the short-time or β-relaxation of the colloids. Attempts to force fit MCT to the dataset produced negative fitting parameters. Furthermore, at $\phi = 0.45$, the values of G'' are always greater than G', indicating that the suspension is fluidlike within the observable frequency range. Although we observe hints of a crossover for rough colloids at $\omega = 0.1$ rad/s, to be conservative, we decided that MCT is not a physically valid model for suspensions with $\Delta\phi/\phi_{max} > 0.20$.

D. Mode-coupling theory analysis for dense suspensions

MCT is best suited for glassy or deeply supercooled systems ($\phi \geq 0.53$, $\Delta\phi/\phi_{max} \leq 0.17$) where a separation between short-time and long-time relaxation can be

measured. For these dense suspensions, the caging effect by the neighboring particles contributes to the increased short- and long-time relaxation as $\phi \to \phi_c$. The consequence of this transient caging effect is kinetically arrested dynamics and an increased viscoelasticity in the suspension (Figs. 3 and 4). The linear viscoelastic behavior of colloidal suspensions approaching the glass transition [28,40,43] has been previously modeled using a version of MCT that sums the high-frequency lubrication hydrodynamic contributions [24] and the glassy elastic contributions [20]. We use this framework to model the G' and G'' of our colloidal suspensions with respect to their relaxation time scales,

$$G'(\omega) = G'_P + G_\sigma\left[\Gamma(1-a')\cos\left(\frac{\pi a'}{2}\right)(\omega t_\sigma)^{a'} - B\Gamma(1+b')\cos\left(\frac{\pi b'}{2}\right)(\omega t_\sigma)^{-b'}\right] + G'_D(\omega), \quad (3)$$

$$G''(\omega) = G_\sigma\left[\Gamma(1-a')\sin\left(\frac{\pi a'}{2}\right)(\omega t_\sigma)^{a'} + B\Gamma(1+b')\sin\left(\frac{\pi b'}{2}\right)(\omega t_\sigma)^{-b'}\right] + G''_D(\omega) + \eta_\infty\omega. \quad (4)$$

In this formulation, the complex modulus is a sum of the microstructural contribution of the glassy cages, the stresses imparted by entropic diffusion, and the pure viscous dissipation in the suspension. The glassy plateau modulus G'_p is a parameter that describes the frequency independent contribution from the structure of the cages, while the gamma functions around the parameters in G_σ ($a' = 0.301$, $b' = 0.545$, and $B = 0.963$ for hard sphere suspensions [28]) describe the near-glass density fluctuations and stress autocorrelation from caging dynamics. Within the viscoelastic G_σ term, t_σ is a parameter for the time scale associated with the G'' minima that separates the short- and long-time relaxation of colloidal glasses [44]. The analytical form of the high-frequency diffusional boundary layer contributions to the complex modulus is given by [24]

$$G'_D(\omega) \approx G''_D(\omega) = \frac{6}{5\pi}\frac{k_BT}{a_{\text{eff}}^3}\phi^2 g(1)\sqrt{\omega\tau_D}, \quad (5)$$

where $g(r/2a_{\text{eff}} = 1) = g(1)$ is the magnitude of the pair distribution function at contact, k_B is Boltzmann's constant, and T is the temperature. The relaxation time scale is defined as $\tau_D = a_{\text{eff}}^2/D_s$, where D_s is the ϕ-dependent short-time diffusivity of hard sphere suspensions [4]. To obtain D_s for the suspensions in this study, we use the relation $D_s/D_0 = \eta_s/\eta_\infty$ [26], where η_s is the solvent viscosity and η_∞ is the high-frequency suspension viscosity. In the theoretical derivation by Lionberger and Russel, integrating the conservation equation using the boundary condition of particles at contact generates a high-frequency storage modulus that scales with $g(1)$. For linear oscillatory perturbations below the yield strain, it is valid to assume that the suspension is near equilibrium. Because $g(1)$ is not well defined in experimental systems, especially for rough particles where the Carnahan–Starling equation of state [45] cannot be used, the mean contact number $\langle z\rangle$ reported for smooth and rough colloids in our earlier work [29] is used as a proxy for $g(1)$. Parameters used for the MCT model are available in Table I.

The high-frequency suspension viscosity term, η_∞, also enters the loss modulus. Figure 7 shows the real part η' of the complex viscosity η^*, defined as G''/ω, as a function of ω where $\lim_{\omega\to\infty}[G''(\omega)/\omega] = \eta_\infty$. The values of η_∞ are obtained using two different methods depending on ϕ. At $\phi < \phi_c$, the

TABLE I. Fit parameters for the mode-coupling theory.

Type	ϕ	G_p (Pa)	G_σ (Pa)	t_σ (s)	D_s (m^2/s)	$\langle z\rangle$	η_∞ (Pa s)
Smooth	0.53	0.005	0.0009	50 000	2.23×10^{-15}	2.5	0.12
	0.55	0.009	0.002	10 000	1.62×10^{-15}	3.5	0.18
	0.58	0.04	0.02	9 000	1.27×10^{-15}	5.0	0.23[a]
	0.61	0.10	0.035	8 000	6.06×10^{-16}	5.5	0.48[a]
	0.62	0.20	0.07	5 000	4.04×10^{-16}	5.8	0.72[a]
Rough	0.50	0.008	0.015	25 000	1.77×10^{-15}	2.0	0.17
	0.52	0.16	0.02	10 000	1.15×10^{-15}	3.0	0.26
	0.53	250	2	5	7.52×10^{-16}	4.0	0.40
	0.55	560	28	4	—	—	—
	0.56	1050	80	1	—	—	—
ω–ϕ superposition	—	0.29	0.01	1.00×10^{6}	1.60×10^{-15}	6.0	0.20

[a]From Eq. (7).

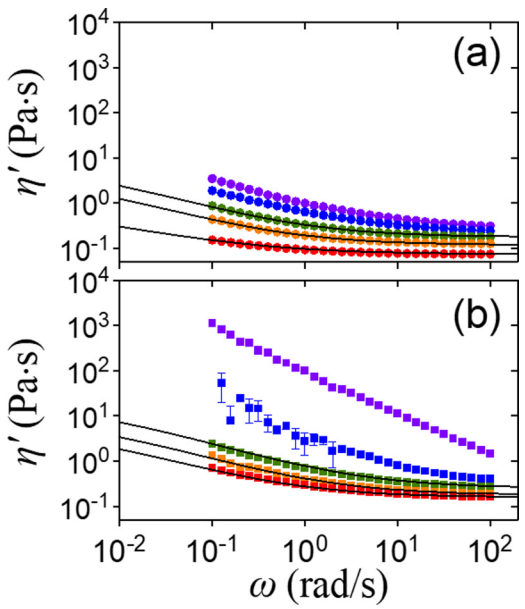

FIG. 7. Real part of the complex viscosity η' from linear viscoelasticity of (a) smooth (circles) and (b) rough colloids (squares) as a function of ω. Solid lines are Cross model fits to the experimental data. Smooth colloid volume fractions are $\phi = 0.45$ ($\Delta\phi/\phi_{\max} = 0.30$, red), $\phi = 0.53$ ($\Delta\phi/\phi_{\max} = 0.18$, orange), $\phi = 0.55$ ($\Delta\phi/\phi_{\max} = 0.14$, green), $\phi = 0.58$ ($\Delta\phi/\phi_{\max} = 0.09$, blue), and $\phi = 0.62$ ($\Delta\phi/\phi_{\max} = 0.03$, purple). Rough colloid volume fractions are $\phi = 0.45$ ($\Delta\phi/\phi_{\max} = 0.21$, red), $\phi = 0.50$ ($\Delta\phi/\phi_{\max} = 0.12$, orange), $\phi = 0.52$ ($\Delta\phi/\phi_{\max} = 0.09$, green), $\phi = 0.53$ ($\Delta\phi/\phi_{\max} = 0.07$, blue), and $\phi = 0.56$ ($\Delta\phi/\phi_{\max} = 0.02$, purple).

Cross model is used to obtain η_∞ from the complex viscosity η' [46,47],

$$\eta' = \frac{\eta_0 - \eta_\infty}{1 + (k\dot{\gamma})^m} + \eta_\infty. \tag{6}$$

The parameters η_0, k, and m are fitting values, where η_0 is the zero-shear viscosity, k is the critical time scale for the onset of shear thinning, and m is the shear thinning power. Table II provides a list of parameters used in the Cross model fitting. Since the experiments involve minimal disturbance of the microstructure in small amplitude frequency sweep experiments, a Cox–Merz relationship of the form $\eta'(\dot{\gamma}) = \eta'(2\pi/\omega)$ is assumed in Eq. (6).

For both smooth and rough colloids at $\phi \geq \phi_c$, but especially for rough colloids, there is no easy way to determine η_∞ or η_0 because of the presence of a yield stress. Instead, an empirical expression is used to obtain the value of η_∞ for smooth colloids. This second order truncated formulation captures the mean-field mobility reduction and an associated increase in viscous dissipation as a function of ϕ [24],

$$\eta_\infty = \eta_s \frac{1 + 1.5\phi(1 + \phi - 0.189\phi^2)}{1 - \phi(1 + \phi - 0.189\phi^2)}, \tag{7}$$

where $\eta_s = 0.012$ Pa s is the squalene viscosity. For rough colloids at $\phi \geq \phi_c$, the material behaves as a glassy material with a well-defined G' and G'' plateau, unlike that of smooth colloids (Figs. 3 and 4). Equations (3)–(7) allow us to capture the complete linear viscoelastic behavior of smooth and rough colloids in our study. Overall, the model provides a good fit to the experimental data as shown in Fig. 8.

E. Frequency-concentration superposition and associated shift parameters

Figure 9 shows the frequency sweep data for the colloidal suspensions for $\phi \geq 0.50$ collapsed onto a single master curve by ω–ϕ superposition. The ω–ϕ superposition is analogous to the time-temperature superposition principle for polymers [48], which allows the mapping of the complex modulus for viscoelastic polymers at different temperatures by assuming that the modulus dependence of the curves on the applied frequency does not change. This principle has been previously extended to colloidal systems [49–51] to elucidate the effect of volume fraction on the caging mechanism responsible for the relaxation of suspensions.

TABLE II. Cross model fit parameters.

Type	ϕ	η_0 (Pa s)	η_∞ (Pa s)	k (s)	M
Smooth	0.45	1	0.08	750	0.55
	0.53	4.5	0.12	500	0.65
	0.55	8	0.18	400	0.65
	0.45	6	0.16	400	0.65
	0.5	10	0.16	250	0.65
	0.52	20	0.26	250	0.65
Rough	0.53	—	0.40[a]	—	—
	0.55	—	1.48[a]	—	—

[a]At $\omega = 100$ rad/s.

To rescale the viscoelastic spectrum, smooth colloids suspended at $\phi = 0.62$ is used as the reference system. The remainder of the data for both smooth and colloids is shifted in the horizontal and vertical axes with respect to the reference system to generate a master curve that represents a glassy material that can be fit to the MCT formulation in Eqs. (3)–(5) [40,50]. Parameters A and B represent the shift factors for the complex modulus and the applied frequency and span 6 and 8 orders of magnitude, respectively. The shifted viscoelastic spectrum is in good agreement with the MCT formulation, using adjustable parameters that are different from that of the individual suspensions (Table I).

A physical description of these shift factors can be obtained in terms of the relaxation time and caging length scales in dense suspensions. Figure 10(a) shows that $A > 1$ for smooth colloids at $\phi < 0.62$ and rough colloids at $\phi < 0.52$, while $A \ll 1$ for rough colloids at $\phi \geq 0.53$. The value of this shift factor indicates how complex modulus differs from the reference system (smooth colloids at $\phi = 0.62$). The complex modulus is a combination of G', which is related to the elastic energy stored in a microstructural cage, and G'', which represents the viscous contributions from solvent interactions between colloids that form the cage. Any shifts in G' and G'', therefore, represent the in-cage displacement and scale as the inverse volume of the cage, again with respect to the reference system. In other words, $A > 1$ means that the unscaled G' and G'' values for the suspension are small and that the caging volume is large. On the other hand, $A \ll 1$ indicates an extremely small caging volume, as seen in rough colloids at $\phi \geq 0.53$; a particle is dynamically arrested within its cage due to steric hindrance from nearest neighbors. Large stresses would be required to perturb the equilibrium microstructure and to overcome the near-field viscous dissipation found in the small lubrication gaps.

The horizontal shift factor B can be thought of as a time scale for a particle to escape from the neighboring cages as suspension ϕ increases [49]. To support this statement, we find that the values of B increase with increasing t_σ (MCT fitting parameters in Table I), suggesting that the separation of short-time and long-time relaxation is correlated with the cage relaxation time of the systems. Figure 10(b) shows values of $B > 1$ for smooth suspensions of $\phi < 0.62$, indicating that these suspensions relax more rapidly because less time is required for particles to escape the larger cage volumes. It is also interesting to note that rough colloids at $0.45 < \phi < \phi_c$ have similar values of B as the reference system, but when the particle loading is at $\phi_c < \phi < \phi_{max}$, then values of B become six orders of magnitude lower than the smooth colloids at all ϕ as well as the rough colloids at $\phi < \phi_c$. This suggests that the time required for a rough colloid to escape from its cage microstructure at $\phi \geq \phi_c$ is nearly six orders of magnitude higher than that of its smooth counterpart at $\phi \geq \phi_c$.

In small amplitude oscillatory rheology, weak flows change the equilibrium pair distribution function $g(r)$ as a first order perturbation that scales with the short-time

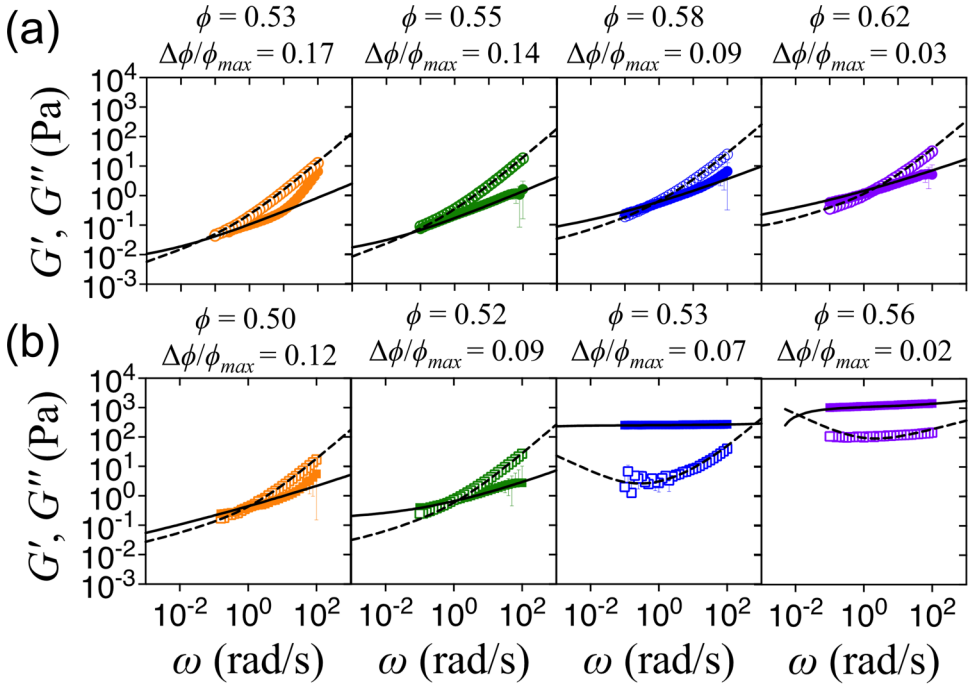

FIG. 8. Fitting experimental data to the mode-coupling theory. Frequency sweep data for suspensions of (a) smooth and (b) rough colloids at different ϕ and $\Delta\phi/\phi_{\max}$. Solid lines represent G', and dashed lines represent G'' from MCT fit.

translational self-diffusivity $D_s \sim g(r)(1 - D_s^{-1})$ [52]. Earlier work has shown that the value of $D_s(\phi)$ for rough colloids is reduced [9] and, hence, the distortion to $g(r)$ may be slightly less pronounced than that of smooth colloids. Furthermore, when $\phi > 0.30$, the effect of surface roughness on the short-time rotational self-diffusivity D_r for rough colloids is an order of magnitude smaller than that of smooth particles at same ϕ [10]. These observations suggest that the thermodynamic and hydrodynamic contributions to G' are enhanced for rough colloids between ϕ_c and $\phi_{\max}$. The large decreases in the shift factors A and B, along with our previous measurements of the rotational dynamics [10], strongly suggest that the geometric frustration generates smaller, stronger cages that relax extremely slowly and therefore restricts the mobility of colloids. Our results indicate that this type of rotational constraint affects not only the elastic glassy structure but also the viscous dissipation due to enhanced hydrodynamics between asperities.

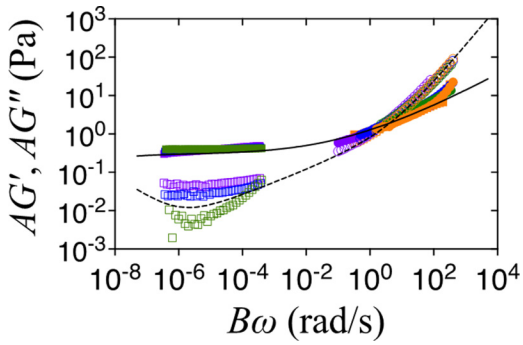

FIG. 9. Frequency-concentration (ω–ϕ) superposition for dense colloidal suspensions. The master curve comprising viscoelasticity data from smooth (circles) and rough (squares) colloids scaled by the horizontal shift factor B and the vertical shift factor A. Reference system is smooth colloids suspended at $\phi = 0.62$. Closed symbols are G', and open symbols are G''. Smooth colloid volume fractions are $\phi = 0.53$ (orange), $\phi = 0.55$ (blue), $\phi = 0.58$ (green), and $\phi = 0.62$ (purple). Rough colloid volume fractions are $\phi = 0.50$ (orange), $\phi = 0.52$ (blue), $\phi = 0.53$ (green), and $\phi = 0.56$ (purple). The solid line represents G', and the dashed line represents G'' from MCT fit.

F. Kinetic description of the glassy modulus

To estimate the localization length of cages formed by rough colloids at $\phi \geq \phi_c$, we plot the scaled localization length scale as a function of $\Delta\phi/\phi_{max}$. Figure 11(a) shows r_L normalized by the effective particle diameter as a function of ϕ. As expected, the localization length scale for rough colloids is nearly 2 orders of magnitude lower than that of the smooth colloids, indicating that particles rattle around in a much smaller cage volume. For rough colloids, the computed localization length approaches ~0.1 nm, suggesting that the polymer brushes may interpenetrate one another and furthermore become significantly compressed. However, we do not have direct evidence of brush compression and the difference between the localization length scales represents a qualitative method way to interpret the geometric frustration created by the rotational constraint in the rough colloids. The localization length scales with cage volume as $r_L \sim V_{\text{cage}}^{1/3}$ and Fig. 11(a) suggests that the space available for smooth particles to rattle is more than that of rough colloids, $V_{\text{cage,s}} > V_{\text{cage,R}}$. However, Fig. 12 suggests that the cage volume for both types of particles should be similar, if we naively consider that rough colloids have the same $2a_{\text{eff}}$ as the smooth colloids. In reality, we suspect that the two orders of magnitude change in is a reflection of the reduced free volume available to rough colloids due to asperity interlocking. This is in qualitative agreement with Fig. 10(a), where rough colloids

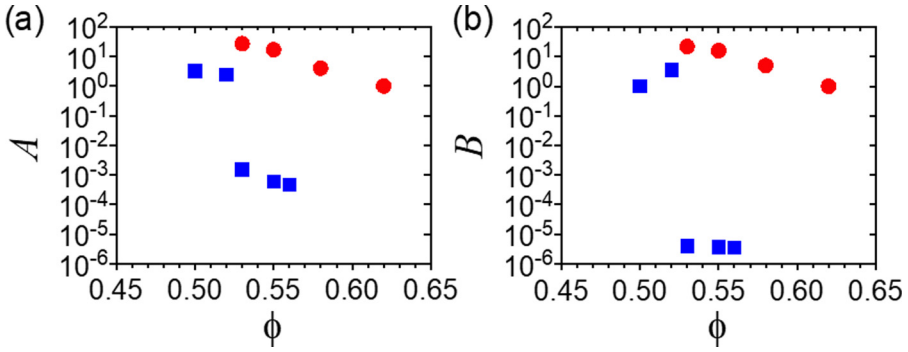

FIG. 10. Shift factors in ω–ϕ superposition. (a) The vertical and (b) horizontal shift factors as a function of ϕ for smooth (red circles) and rough (blue squares) colloids.

displayed a three orders-of-magnitude reduction in the shift factor A. In addition, dynamic localization theory states that the hopping energy barrier E_B scales with r_L as $E_B \sim k_B T(a_{eff}/r_L)$ [23]. This gives an estimate of E_B as $\sim 10^4\, k_B T$ for rough colloids and $\sim 10^2\, k_B T$ for smooth colloids at $\phi \geq \phi_c$. If we assume that the associated cage escape time scale has an Arrhenius type scaling of $\tau_B \sim \exp(-E_B)$, then it would take rough colloids almost infinitely longer to escape their glassy cages than smooth colloids near maximum packing.

The difference in the localization lengths and cage escape times can be related to G_P' within the context of the activated hopping theory, which links r_L at the single-particle level and glassy dynamics at $\phi \geq \phi_c$ in the ultralocal limit as [23,53,54]

$$G_P' \cong \frac{9}{5\pi}\frac{\phi k_B T}{a_{eff} r_L^2}. \tag{8}$$

For $\phi_c > \phi > \phi_{max}$, we obtain localization length scale r_L for suspensions of smooth and rough colloidal suspensions from the respective G_P' and ϕ values. Figure 11(b) shows the scaled glassy modulus as a function of the distance from jamming. To compare our data with the activated hopping theory, we use an empirical form of the hard sphere localization length as $r_L = 29.9 a_{eff} \exp(-12.2\phi)$ [54]. This empirical description is in good agreement with experimental data for the smooth colloids at $\phi \geq \phi_c$. The glassy modulus increases as the volume fraction approach the respective ϕ_{max}, as expected. The values of G_p' for rough colloids are plotted for comparison, but there is currently no prediction or empirical data for how r_L varies with ϕ for rough colloids.

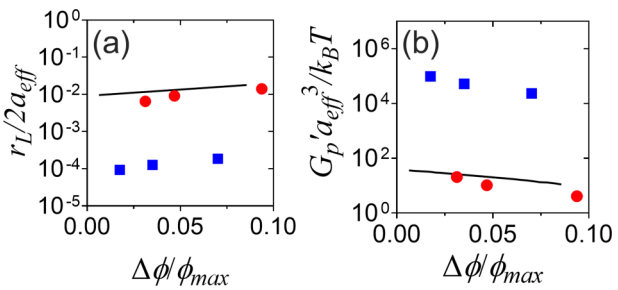

FIG. 11. Glassy dynamics and kinetic theory. (a) The scaled localization length as a function of ϕ. The solid line represents the hard sphere-prediction from the activated hopping theory. (b) The scaled glassy modulus as a function of the distance from Solid lines represent empirical correlations for hard spheres in Ref. 54. Experimental data for smooth (red circles) and rough (blue squares) colloids are shown.

G. Evidence for enhanced lubrication between asperities from high-frequency moduli

The high-frequency dependence of G' and G'' is commonly used to evaluate the relative contributions of hydrodynamic and interparticle forces to the suspension stress because the oscillations introduce affine perturbations in such a rapid manner that the microstructure is unable to relax its shear-induced anisotropy through the Brownian motion [24,26,27,55]. As $\omega \to \infty$, the contributions to suspension stress become dominated by the lubrication stresses of the solvent between neighboring particles. High-frequency oscillatory methods have been previously used to extract the viscous and elastic stresses for hairy PMMA colloids and raspberrylike silica colloids [2]. In our rheological experiments, we define the high-frequency limit as the value of ω at which η' approaches η_∞ [24], corresponding to $\omega \geq 10$ rad/s. The Brownian diffusion time scales of smooth and rough colloids at infinite dilution, $t_D = a_{eff}^2/D_0 = 6\pi\eta_s a_{eff}^3/(k_B T)$, are between 23 and 26 s and correspond to a characteristic frequency range between 0.2 and 0.3 rad/s. The choice of $\omega = 10$ rad/s as the high-frequency limit is, therefore, acceptable, especially considering that dense suspensions relax 1–2 orders of magnitude more slowly than dilute suspensions. Note that our experimental time scale is far from the inertial relaxation and vorticity diffusion times of the PMMA colloids, defined as $t_i = a_{eff}^2 \rho_{PMMA}/18\eta_s$ and $t_v = a_{eff}^2 \rho_{PMMA}/\eta_s$, respectively. At $\omega = 10$ rad/s, the oscillatory time scale is $\sim 10^{-1}$ s while t_i and t_v are $\sim 10^{-8}$ and $\sim 10^{-9}$ s, indicating that particle inertia is unimportant in our study.

Figure 12 shows that at $\phi \geq \phi_c$, the high-frequency storage modulus G'_∞ for both smooth and rough particles are on the same order of magnitude at $\phi \leq 0.52$. At $\phi > 0.52$, rough colloids exhibit G'_∞ nearly 10^3 times that of the smooth colloids. In addition, G'_∞ scales with $\omega^{1/2}$ for smooth colloids, corresponding to the free-draining approximation between hard spheres [24]. In contrast, G'_∞ is frequency independent for rough colloids. This type of transition from free-draining to fully lubricated behavior was previously observed in hairy

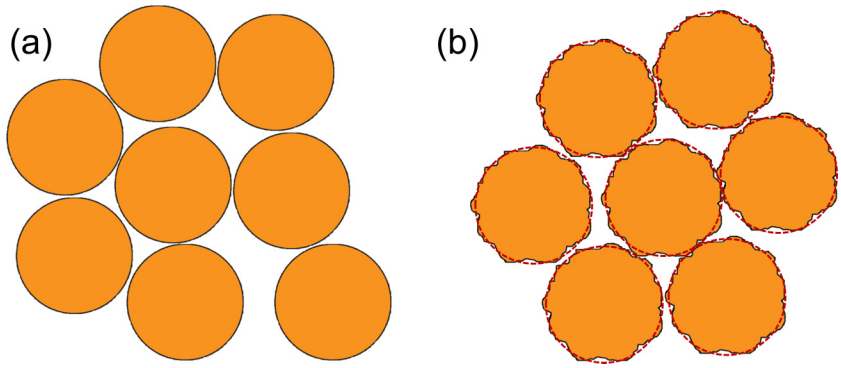

FIG. 12. Microstructural visualization of glassy cages formed by (a) smooth and (b) rough colloids. On first glance, approximating the rough colloids with an effective spherical shape with the same diameter as the smooth colloids (red dashed lines) suggests that there should be little difference in their cage volumes. In reality, data presented in this study and elsewhere [10] state that there is a significant difference in their cage volumes; this could be possible if we consider the geometric overlapping and interlocking between very rough asperities. The steric layer is not shown here.

PHSA-PMMA and raspberrylike silica colloids [2]. Schroyen *et al.* altered the PHSA brush contour length on the PHSA-PMMA colloids, finding that PMMA colloids with longer stabilizer brushes (60 nm) exhibited $G'_\infty \sim \omega^{1/2}$, whereas very thin brush layers (6 nm) led to $G'_\infty \sim \omega^0$. This phenomenon was attributed to the free flow of solvent in long brushes that screened out strong lubrication forces until the brushes became compressed, while thin brushes were less effective at hydrodynamic screening and exhibited a weak power-law dependence. Interestingly, they also noted a significant increase in both the elastic and viscous stresses in suspensions of raspberrylike silica colloids at intermediate ω, and that the effective thickness of the diffusional boundary layer was equivalent to the roughness length scale.

In our experimental data (Fig. 13), suspensions of smooth colloids obey the free-draining approximation for all ϕ, suggesting that our PHSA stabilizer layers are potentially compressible. Crucially, suspensions of rough particles follow a similar free-draining trend up to ϕ_c, and then full lubrication becomes prominent at $\phi \geq \phi_c$, possibly because of interlocking between the rough facets of neighboring particles. These observations agree with the data for raspberrylike silica from Schroyen *et al.*, with the exception that we find a significant change in the lubrication behavior for rough colloids at $\phi/\phi_{max} \geq 0.93$. We attribute these differences to the type of interactions present in our system. At $\phi < \phi_c$, both rough and smooth colloids generate "soft" contacts due to the compressibility of PHSA brushes in a way that fits the diffusion boundary layer mechanism. At low values of ω, diffusion is still capable of relaxing the nonequilibrium microstructure. The "hard" lubricated contacts are found only at $\phi \geq \phi_c$ as $\phi \to \phi_{max}$, where asperities in near contact leads to a much stronger contribution to the suspension stress from squeeze flows. The shift from the diffusional to lubrication layers is only observed for the rough colloids possibly because of extreme asperity-asperity hydrodynamic interactions, which manifest as additional gap-dependent terms in the hard sphere-lubrication squeeze force [19].

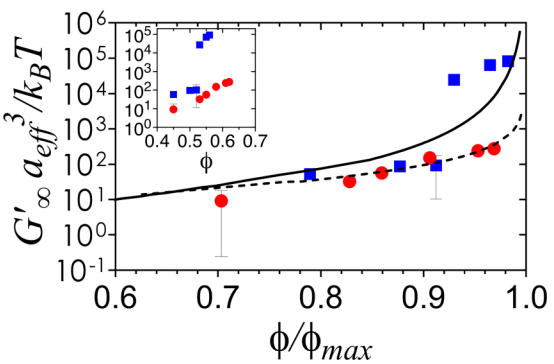

FIG. 13. Scaled G'_∞ as a function of scaled ϕ. The solid line represents prediction from the hydrodynamic boundary layer theory, and the dashed line represents prediction from free-draining approximation. Experimental data for smooth (red circles) and rough (blue squares) colloids at $\omega = 10$ rad/s are shown. *Inset*: Scaled G'_∞ as a function of ϕ.

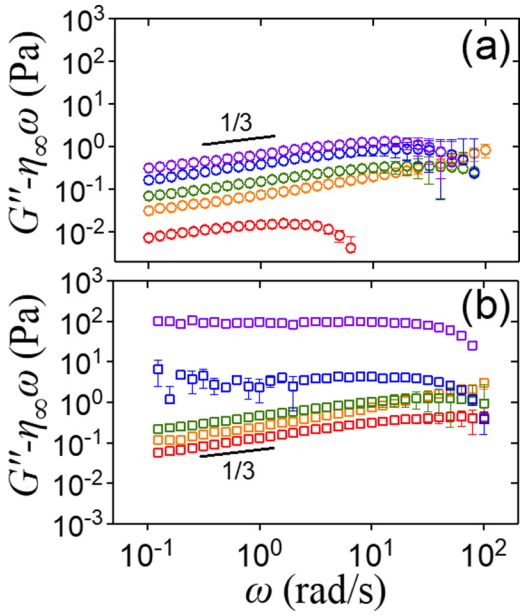

FIG. 14. Loss modulus without solvent contributions. Experimental data for (a) smooth and (b) rough colloids are shown as a function of ω. Smooth colloid volume fractions are $\phi = 0.45$ ($\Delta\phi/\phi_{max} = 0.30$, red), $\phi = 0.53$ ($\Delta\phi/\phi_{max} = 0.18$, orange), $\phi = 0.55$ ($\Delta\phi/\phi_{max} = 0.14$, green), $\phi = 0.58$ ($\Delta\phi/\phi_{max} = 0.09$, blue), and $\phi = 0.62$ ($\Delta\phi/\phi_{max} = 0.03$, purple). Rough colloid volume fractions are $\phi = 0.45$ ($\Delta\phi/\phi_{max} = 0.21$, red), $\phi = 0.50$ ($\Delta\phi/\phi_{max} = 0.12$, orange), $\phi = 0.52$ ($\Delta\phi/\phi_{max} = 0.09$, green), $\phi = 0.53$ ($\Delta\phi/\phi_{max} = 0.07$, blue), and $\phi = 0.56$ ($\Delta\phi/\phi_{max} = 0.02$, purple).

We further note that the loss modulus exhibits unusual dependences on ϕ for rough colloids at the highest volume fractions tested. Figure 4 shows that rough colloids exhibit large increases in G'' when $\phi \geq 0.53$, in ways that are not seen with smooth colloids. A local minimum in G'' is observed at $\phi = 0.53$, which is characteristic of glassy behavior in dense colloidal suspensions [49]. Surprisingly, no such minimum is found when $\phi \geq 0.56$, and both G' and G'' exhibit nearly complete frequency independence. The ω-independence of G'' is normally found in gelling materials that comprise of rigid networks formed by adhesive colloids [56] but have not been observed in glassy hard sphere systems. Removing the bulk solvent contribution $\eta_\infty\omega$ from G'', as shown in Fig. 14, more accurately represents the viscous contribution from particle-particle and asperity-asperity interactions. Smooth colloids at all ϕ display a weak power-law scaling of $(G'' - \eta_\infty\omega) \sim \omega^{1/3}$ at low ω, followed by a sharp drop in G''. This behavior is consistent with hard sphere systems [26]. Rough colloids exhibit similar $(G'' - \eta_\infty\omega)$ scalings at $\phi < 0.53$, but the behavior at low ω becomes frequency independent at $\phi \geq 0.53$. The average value of $(G'' - \eta_\infty\omega)$ at $\phi = 0.53$ is about an order of magnitude larger than that at $\phi = 0.52$, and this difference becomes three orders of magnitude larger at $\phi = 0.56$. In contrast, $(G'' - \eta_\infty\omega)$ does not increase significantly with ϕ for smooth colloids. These results suggest that the hydrodynamic interactions between rough colloids are different from that of smooth colloids, and that load-bearing networks could be formed by strong lubrication forces at $\phi = 0.56$ by interlocking asperities that relax extremely slowly due to hindered rotations [10,19]. Although these near-equilibrium microstructures bear resemblance to the hydroclusters and force chains found in shear thickening suspensions [15,16], the physical origins of the suspension stresses in both cases could be rather different.

IV. CONCLUSIONS

We investigate the effect of surface roughness on the linear viscoelastic rheology of colloids in dense suspensions. Suspensions of rough colloids exhibit viscoelastic moduli, G' and G'', that are orders of magnitude higher than suspensions of smooth colloids. A physical interpretation for this observation is that the rough facets between nearest neighbors interlock when the surface separation is small at high densities ($\phi_c < \phi < \phi_{max}$), which causes a large increase in the near-field hydrodynamics and reduces the effective free volume available for the rough colloids to relax within the suspensions. The experimental data are compared against theories of mode-coupling, activated barrier hopping, and high-frequency boundary layers. The analyses provide evidence that rough colloids in dense suspensions create stress-bearing networks that are reminiscent of the clusters and networks in shear thickening suspensions, but instead operate primarily through strong lubrication interactions between asperities on the surface of the rough colloids.

This work provides a mean-field description of how roughness-induced geometric frustration modifies the spatio-temporal scales responsible for the viscoelastic response of hard-particle suspensions at high ϕ. The microstructural and dynamical parameters obtained from theoretical modeling provide an additional inference of the small structural perturbations and glassy behavior of these suspensions. Although there is no real-time microstructural characterization in this study, earlier work indicates that slow clusters contribute to the bulk elasticity in dense colloidal glasses [57]. It would be interesting in the future to visualize single-particle dynamics using confocal rheometry, which could reveal clusters with correlated dynamics in dense suspensions of rough colloids. This would enable a greater understanding of the slow flows caused by rough particles in geophysical phenomena and cement [12] or enhance the properties of colloidal composite materials used as impact-resistant textiles and coatings [58].

ACKNOWLEDGMENTS

The authors thank Jan Vermant, James Swan, and Jeffrey Morris for scientific discussions. This work is supported by the International Fine Particles Research Institute (No. 129-CA), the National Science Foundation (Nos. CBET-1804462 and DMR-2104726), and the American Chemical Society Petroleum Research Fund (No. 59208-DNI9).

AUTHOR DECLARATIONS

Conflict of Interest

The authors have no conflicts to disclose.

REFERENCES

[1] Hsiao, L. C., and S. Pradeep, "Experimental synthesis and characterization of rough particles for colloidal and granular rheology," Curr. Opin. Colloid Interface Sci. **43**, 94–112 (2019).

[2] Schroyen, B., C.-P. Hsu, L. Isa, P. Van Puyvelde, and J. Vermant, "Stress contributions in colloidal suspensions: The smooth, the rough, and the hairy," Phys. Rev. Lett. **122**, 218001 (2019).

[3] Russel, W. B., D. A. Saville, and W. R. Schowalter, *Colloidal Dispersions* (Cambridge University, Cambridge, 1989).

[4] Brady, J. F., "The rheological behavior of concentrated colloidal dispersions," J. Chem. Phys. **99**, 567–581 (1993).

[5] Brady, J. F., "The long-time self-diffusivity in concentrated colloidal dispersions," J. Fluid Mech. **272**, 109–134 (1994).

[6] Phillips, R. J., J. F. Brady, and G. Bossis, "Hydrodynamic transport properties of hard-sphere dispersions. I: Suspensions of freely mobile particles," Phys. Fluids **31**, 3462–3472 (1988).

[7] Yanagishima, T., Y. Liu, H. Tanaka, and R. P. A. Dullens, "Particle-level visualization of hydrodynamic and frictional couplings in dense suspensions of spherical colloids," Phys. Rev. X **11**, 021056 (2021).

[8] Roller, J., A. Laganapan, J.-M. Meijer, M. Fuchs, and A. Zumbusch, "Observation of liquid glass in suspensions of ellipsoidal colloids," Proc. Natl. Acad. Sci. U.S.A. **118**, e2018072118 (2021).

[9] Ilhan, B., F. Mugele, and M. H. G. Duits, "Roughness induced rotational slowdown near the colloidal glass transition," J. Colloid Interface Sci. **607**, 1709–1716 (2022).

[10] Hsiao, L. C., I. Saha-Dalal, R. G. Larson, and M. J. Solomon, "Translational and rotational dynamics in dense suspensions of smooth and rough colloids," Soft Matter **13**, 9229–9236 (2017).

[11] Bi, D., X. Yang, M. C. Marchetti, and M. L. Manning, "Motility-driven glass and jamming transitions in biological tissues," Phys. Rev. X **6**, 021011 (2016).

[12] Ferdowsi, B., C. P. Ortiz, and D. J. Jerolmack, "Glassy dynamics of landscape evolution," Proc. Natl. Acad. Sci. U.S.A. **115**, 4827–4832 (2018).

[13] Jamali, S., and J. F. Brady, "Alternative frictional model for discontinuous shear thickening of dense suspensions: Hydrodynamics," Phys. Rev. Lett. **123**, 138002 (2019).
[14] Otsuki, M., and H. Hayakawa, "Discontinuous change of shear modulus for frictional jammed granular materials," Phys. Rev. E **95**, 062902 (2017).
[15] Pradeep, S., M. Nabizadeh, A. R. Jacob, S. Jamali, and L. C. Hsiao, "Jamming distance dictates colloidal shear thickening," Phys. Rev. Lett. **127**, 158002 (2021).
[16] Hsu, C.-P., S. N. Ramakrishna, M. Zanini, N. D. Spencer, and L. Isa, "Roughness-dependent tribology effects on discontinuous shear thickening," Proc. Natl. Acad. Sci. U.S.A. **115**, 5117–5122 (2018).
[17] Rice, R., R. Roth, and C. P. Royall, "Polyhedral colloidal 'rocks': Low-dimensional networks," Soft Matter **8**, 1163–1167 (2012).
[18] Singh, A., C. Ness, R. Seto, J. J. de Pablo, and H. M. Jaeger, "Shear thickening and jamming of dense suspensions: The 'roll' of friction," Phys. Rev. Lett. **124**, 248005 (2020).
[19] Wang, M., S. Jamali, and J. F. Brady, "A hydrodynamic model for discontinuous shear-thickening in dense suspensions," J. Rheol. **64**, 379–394 (2020).
[20] Gotze, W., and L. Sjogren, "Relaxation processes in supercooled liquids," Rep. Prog. Phys. **55**, 241–376 (1992).
[21] Brader, J. M., T. Voigtmann, M. Fuchs, R. G. Larson, and M. E. Cates, "Glass rheology: From mode-coupling theory to a dynamical yield criterion," Proc. Natl. Acad. Sci. U.S.A. **106**, 15186–15191 (2009).
[22] Bouchaud, J.-P., L. Cugliandolo, J. Kurchan, and M. Mézard, "Mode-coupling approximations, glass theory and disordered systems," Phys. A **226**, 243–273 (1996).
[23] Schweizer, K. S., and E. J. Saltzman, "Entropic barriers, activated hopping, and the glass transition in colloidal suspensions," J. Chem. Phys. **119**, 1181–1196 (2003).
[24] Lionberger, R. A., and W. B. Russel, "High frequency modulus of hard sphere colloids," J. Rheol. **38**, 1885–1908 (1994).
[25] Fritz, G., B. Maranzano, N. Wagner, and N. Willenbacher, "High frequency rheology of hard sphere colloidal dispersions measured with a torsional resonator," J. Non-Newtonian Fluid Mech. **102**, 149–156 (2002).
[26] Shikata, T., and D. S. Pearson, "Viscoelastic behavior of concentrated spherical suspensions," J. Rheol. **38**, 601–616 (1994).
[27] van der Werff, J. C., C. G. de Kruif, C. Blom, and J. Mellema, "Linear viscoelastic behavior of dense hard-sphere dispersions," Phys. Rev. A **39**, 795–807 (1989).
[28] Mason, T. G., and D. A. Weitz, "Linear viscoelasticity of colloidal hard sphere suspensions near the glass transition," Phys. Rev. Lett. **75**, 2770–2773 (1995).
[29] Pradeep, S., and L. C. Hsiao, "Contact criterion for suspensions of smooth and rough colloids," Soft Matter **16**, 4980–4989 (2020).
[30] Hunter, G. L., and E. R. Weeks, "The physics of the colloidal glass transition," Rep. Prog. Phys. **75**, 066501 (2012).
[31] Crocker, J. C., and D. G. Grier, "Methods of digital video microscopy for colloidal studies," J. Colloid Interface Sci. **179**, 298–310 (1996).
[32] Torquato, S., T. M. Truskett, and P. G. Debenedetti, "Is random close packing of spheres well defined?," Phys. Rev. Lett. **84**, 2064–2067 (2000).
[33] Petekidis, G., D. Vlassopoulos, and P. N. Pusey, "Yielding and flow of sheared colloidal glasses," J. Phys.: Condens. Matter **16**, S3955–S3963 (2004).
[34] Trappe, V., and D. A. Weitz, "Scaling of the viscoelasticity of weakly attractive particles," Phys. Rev. Lett. **85**, 449–452 (2000).
[35] Shih, W.-H., W. Y. Shih, S.-I. Kim, J. Liu, and I. A. Aksay, "Scaling behavior of the elastic properties of colloidal gels," Phys. Rev. A **42**, 4772–4779 (1990).
[36] Mason, T. G., J. Bibette, and D. A. Weitz, "Elasticity of compressed emulsions," Phys. Rev. Lett. **75**, 2051–2054 (1995).
[37] Winter, H. H., and F. Chambon, "Analysis of linear viscoelasticity of a crosslinking polymer at the gel point," J. Rheol. **30**, 367–382 (1986).
[38] Pandey, R., and J. C. Conrad, "Gelation in mixtures of polymers and bidisperse colloids," Phys. Rev. E **93**, 012610 (2016).
[39] Hsiao, L. C., M. J. Solomon, K. A. Whitaker, and E. M. Furst, "A model colloidal gel for coordinated measurements of force, structure, and rheology," J. Rheol. **58**, 1485–1504 (2014).
[40] Crassous, J. J., R. Régisser, M. Ballauff, and N. Willenbacher, "Characterization of the viscoelastic behavior of complex fluids using the piezoelastic axial vibrator," J. Rheol. **49**, 851–863 (2005).
[41] Kramb, R. C., R. Zhang, K. S. Schweizer, and C. F. Zukoski, "Glass formation and shear elasticity in dense suspensions of repulsive anisotropic particles," Phys. Rev. Lett. **105**, 055702 (2010).
[42] Macosko, C. W., *Rheology Principles, Measurements and Applications* (Wiley, New York, NY, 1994).
[43] Daneshfar, Z., F. Goharpey, H. Nazockdast, and R. Foudazi, "Rheology of concentrated bimodal suspensions of nanosilica in PEG," J. Rheol. **61**, 955–966 (2017).
[44] Helgeson, M. E., N. J. Wagner, and D. Vlassopoulos, "Viscoelasticity and shear melting of colloidal star polymer glasses," J. Rheol. **51**, 297–316 (2007).
[45] Sierou, A., and J. F. Brady, "Rheology and microstructure in concentrated noncolloidal suspensions," J. Rheol. **46**, 1031–1056 (2002).
[46] Bergström, L., "Shear thinning and shear thickening of concentrated ceramic suspensions," Colloids Surf., A **133**, 151–155 (1998).
[47] Roberts, G. P., H. A. Barnes, and P. Carew, "Modelling the flow behaviour of very shear-thinning liquids," Chem. Eng. Sci. **56**, 5617–5623 (2001).
[48] Rubenstein, M., and R. H. Colby, *Polymer Physics* (Oxford University, New York, 2003).
[49] Jacob, A. R., A. S. Poulos, S. Kim, J. Vermant, and G. Petekidis, "Convective cage release in model colloidal glasses," Phys. Rev. Lett. **115**, 218301 (2015).
[50] Mattsson, J., H. M. Wyss, A. Fernandez-Nieves, K. Miyazaki, Z. Hu, D. R. Reichman, and D. A. Weitz, "Soft colloids make strong glasses," Nature **462**, 83–86 (2009).
[51] Siebenbürger, M., M. Fuchs, H. Winter, and M. Ballauff, "Viscoelasticity and shear flow of concentrated, noncrystallizing colloidal suspensions: Comparison with mode-coupling theory," J. Rheol. **53**, 707–726 (2009).
[52] Lionberger, R. A., and W. B. Russel, "Microscopic theories of the rheology of stable colloidal dispersions," Adv. Chem. Phys. **111**, 399–474 (1999).
[53] Schweizer, K. S., and G. Yatsenko, "Collisions, caging, thermodynamics, and jamming in the barrier hopping theory of glassy hard sphere fluids," J. Chem. Phys. **127**, 164505 (2007).
[54] Schweizer, K. S., and E. J. Saltzman, "Activated hopping, barrier fluctuations, and heterogeneity in glassy suspensions and liquids," J. Phys. Chem. B **108**, 19729–19741 (2004).
[55] Elliott, S. L., and W. B. Russel, "High frequency shear modulus of polymerically stabilized colloids," J. Rheol. **42**, 361–378 (1998).
[56] Kim, J. M., J. Fang, A. P. Eberle, R. Castañeda-Priego, and N. J. Wagner, "Gel transition in adhesive hard-sphere colloidal dispersions: The role of gravitational effects," Phys. Rev. Lett. **110**, 208302 (2013).
[57] Conrad, J. C., P. P. Dhillon, E. R. Weeks, D. R. Reichman, and D. A. Weitz, "Contribution of slow clusters to the bulk elasticity near the colloidal glass transition," Phys. Rev. Lett. **97**, 265701 (2006).
[58] Decker, M., C. Halbach, C. Nam, N. Wagner, and E. Wetzel, "Stab resistance of shear thickening fluid (STF)-treated fabrics," Compos. Sci. Technol. **67**, 565–578 (2007).